Organic Geochemistry 197 (2024) 104883

Contents lists available at ScienceDirect

Organic Geochemistry

journal homepage: www.elsevier.com/locate/orggeochem

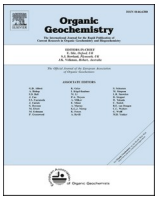

Distribution and origin of higher diamondoids in the ultra-deep Paleozoic condensates of the Shunbei oilfield in the Tarim Basin, NW China

Rongzhen Qiao, Meijun Li *, Donglin Zhang, Hong Xiao

National Key Laboratory of Petroleum Resources and Engineering, College of Geosciences, China University of Petroleum (Beijing), Beijing 102249, China

ARTICLE INFO

Huiyuan Xu - Executive Guest Editor

Keywords:
Higher diamondoids
Hydrothermal alteration
Formation pathway
Tarim Basin

ABSTRACT

Higher diamondoids in the condensates of the Shunbei oilfield were analyzed using GC–MS. The findings indicate that the condensates in the Shunbei oilfield were subjected to a superimposed effect of secondary alterations, including biodegradation, hydrothermal alteration, evaporative fractionation, cracking, and TSR. High local concentrations of thiaadamantanes in oil may result from the interaction of H_2S, derived from Cambrian TSR, with Ordovician hydrocarbons, influenced by hydrothermal activities. Comprehensive analysis shows that TSR is local and limited in Ordovician reservoirs in the Shunbei oilfield and has no significant impact on oil chemistry. Comparative studies indicate that the diamondoid concentrations in condensates from the Shunbei oilfield have not been significantly impacted by biodegradation and evaporative fractionation. Parameters related to diamantanes can effectively characterize their geochemical characteristics and secondary alteration. A multi-parameter correlation heat map suggests that higher diamondoids in the condensates of the Shunbei oilfield are not due to high thermal evolution but have been altered by hydrothermal activity. The hydrothermal activity promotes the formation of higher diamondoids in the condensate. The higher diamondoids that are formed by hydrothermal activity offer a new perspective for studying hydrothermal processes. Additionally, this aids in studying the organic-inorganic interactions of ultra-deep organic fluids with their mineralogical and aqueous environments.

1. Introduction

Diamondoids, characterized by highly symmetrical cage-like molecular structures, are extremely stable (Lin and Wilk, 1995). Diamondoids are classified based on the number of cages into lower diamondoids (≤3 cages) and higher diamondoids (>3 cages) (Lin and Wilk, 1995). Lower diamondoids are widely distributed in oils, particularly in high-mature petroleum (Wingert, 1992). The concentrations of higher diamondoids in petroleum are minute, with concentrations mostly below detection limits (Lin and Wilk, 1995; Wei et al., 2011). The breakthrough in ultra-deep petroleum exploration has led to higher maturity and more complex secondary processes (Chen et al., 2022; Qiao and Chen, 2022). Traditional biomarkers (steranes and terpanes) are significantly reduced by maturity and secondary processes (Graas, 1990). However, relatively stable aromatics cannot provide effective evaluation indexes under the influence of secondary processes (Xu et al., 2024). Both have obvious limitations in characterizing the geochemistry of ultra-deep oils. Due to their unique stability, diamondoids remain present in oils where biomarkers are absent (Qiao et al., 2022). Studies have shown that diamondoid composition is effectively applicable in evaluating organic matter sources, maturity, and secondary alteration (Chen et al., 1996; Schulz et al., 2001; Qiao et al., 2022). This has generated widespread interest in diamondoids, making them a research focus in petroleum geochemistry.

Higher diamondoids, consisting of diamondoid clusters with >3 cages, possess greater thermal stability (Dahl et al., 2003). Their exceptional stability makes higher diamondoids useful in unconventional and ultra-deep oilfield applications (Atwah et al., 2021). Higher diamondoids serve as important indicators in geological evolution, useful in maturity identification, oil-source correlation, and petroleum migration (Scarlett et al., 2019; Atwah et al., 2021). However, since higher diamondoids are observed in samples with higher maturity, most oil samples are below the detection limit without purification (Berwick et al., 2011; Wei et al., 2011). This poses significant challenges to the research and widespread use of higher diamondoids.

This study determined the geochemical characteristics and secondary alteration of the condensate samples from the Shunbei oilfield using higher diamondoids, including tetramantanes, pentamantanes, and

* Corresponding author.
E-mail address: meijunli@cup.edu.cn (M. Li).

https://doi.org/10.1016/j.orggeochem.2024.104883
Received 29 July 2024; Received in revised form 5 October 2024; Accepted 5 October 2024
Available online 10 October 2024

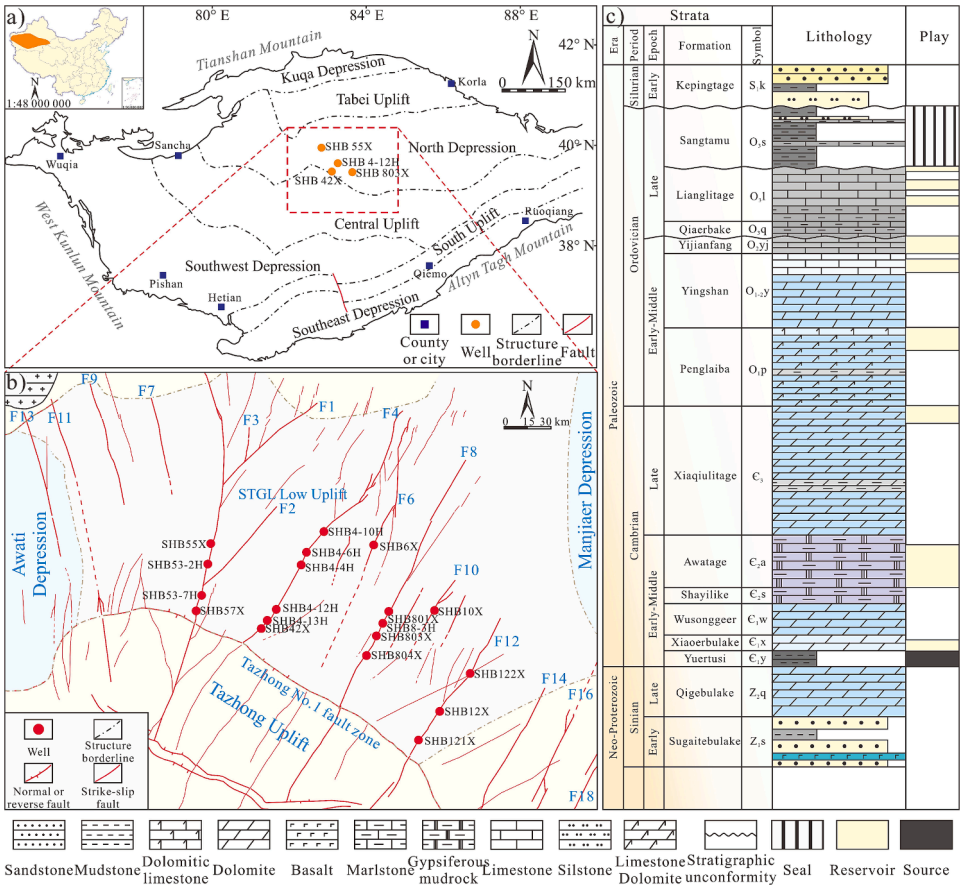

Fig. 1. a) Geological maps showing the location and tectonic units in the Tarim basin; b) Geological maps showing the well location and fault zone distribution in the Shunbei oilfield; c) Simplified stratigraphic column of lower Paleozoic strata in the Shunbei oilfield.

hexamantanes. Based on these findings in combination with the analyses of saturated and aromatic hydrocarbons, lower diamondoids, and thiadiamondoids, the origin and geological significance of higher diamondoids in the Shunbei oilfield condensates are discussed.

2. Geological setting

Tarim Basin, the largest petroliferous basin in China, is renowned for its ultra-deep condensate (Qiao et al., 2024a). It is a typical superimposed basin, consisting of a Paleozoic marine craton basin and a Meso-Cenozoic terrestrial foreland basin (Li et al., 2010a). The stratigraphic filling sequence can be summarized as the Sinian-Devonian marine sedimentary system, the Carboniferous-Permian marine-terrestrial transitional sedimentary system, and the Mesozoic-Cenozoic terrestrial sedimentary system (Wang et al., 2021). After its polycyclic tectonic evolution, the present tectonic pattern of the basin was formed. It is mainly composed of the Southeast Depression, the South Uplift, the Southwest Depression, the Central Uplift, the North Depression, the Tabei Uplift, and the Kuqa Depression as first-order tectonic units (Fig. 1a).

The samples used in this study are primarily from the Shunbei oilfield in the Tarim Basin, which is situated in the Shuntuoguole low uplift (Fig. 1b). The superimposed transformation from multi-stage tectonic movements formed a complex fault system (Fig. 1b). This fault system provides channels for petroleum migration and reservoir spaces for petroleum accumulation (Deng et al., 2022). The mudstone of the Cambrian Yuertusi Formation is the primary source rock for the Paleozoic reservoirs (Fig. 1c). Currently, petroleum exploration in the Shunbei oilfield is concentrated in the Ordovician Yingshan Formation ($O_{1\text{-}2}y$) and Yijianfang Formation (O_2yj) (Fig. 1c).

3. Samples and methods

In this study, eighteen condensates were collected at wellheads in the Shunbei oilfield. The samples were refrigerated before being transported to the laboratory for experimental analysis. Aromatics and organic sulfur compounds (OSCs) were separated using conventional and Ag^+ chromatographic columns, respectively. The Ag^+ chromatographic column preparation and subsequent separation were conducted under light-avoiding conditions. $AgNO_3$ was dissolved in distilled water to prepare a 10 % solution, which was then used to impregnate 200-mesh silica gel. This impregnated gel was activated at 105 °C for 4 h. The separation column was packed with $AgNO_3$-impregnated silica gel, and the oil sample was then added to the Ag^+ chromatographic column. Saturated hydrocarbons, aromatic hydrocarbons, and OSCs were sequentially eluted using *n*-hexane, dichloromethane, and acetone. After solvent evaporation, the samples were concentrated to 5 mg/mL for GC–MS analysis.

3.1. GC

An Agilent 6890GC instrument equipped with an HP-PONA quartz capillary column (50 m × 0.25 mm × 0.25 μm) was utilized for whole-oil analysis. The detailed temperature program was: an initial oven temperature was maintained at 35 °C for 10 min, increased to 60 °C at 0.5 °C/min, then to 300 °C at 2 °C/min, and held for 10 min.

3.2. GC–MS

Agilent 6890 GC and Agilent 5975i MS were used for the GC–MS analysis of condensate, aromatics, and OSCs. The GC was equipped with

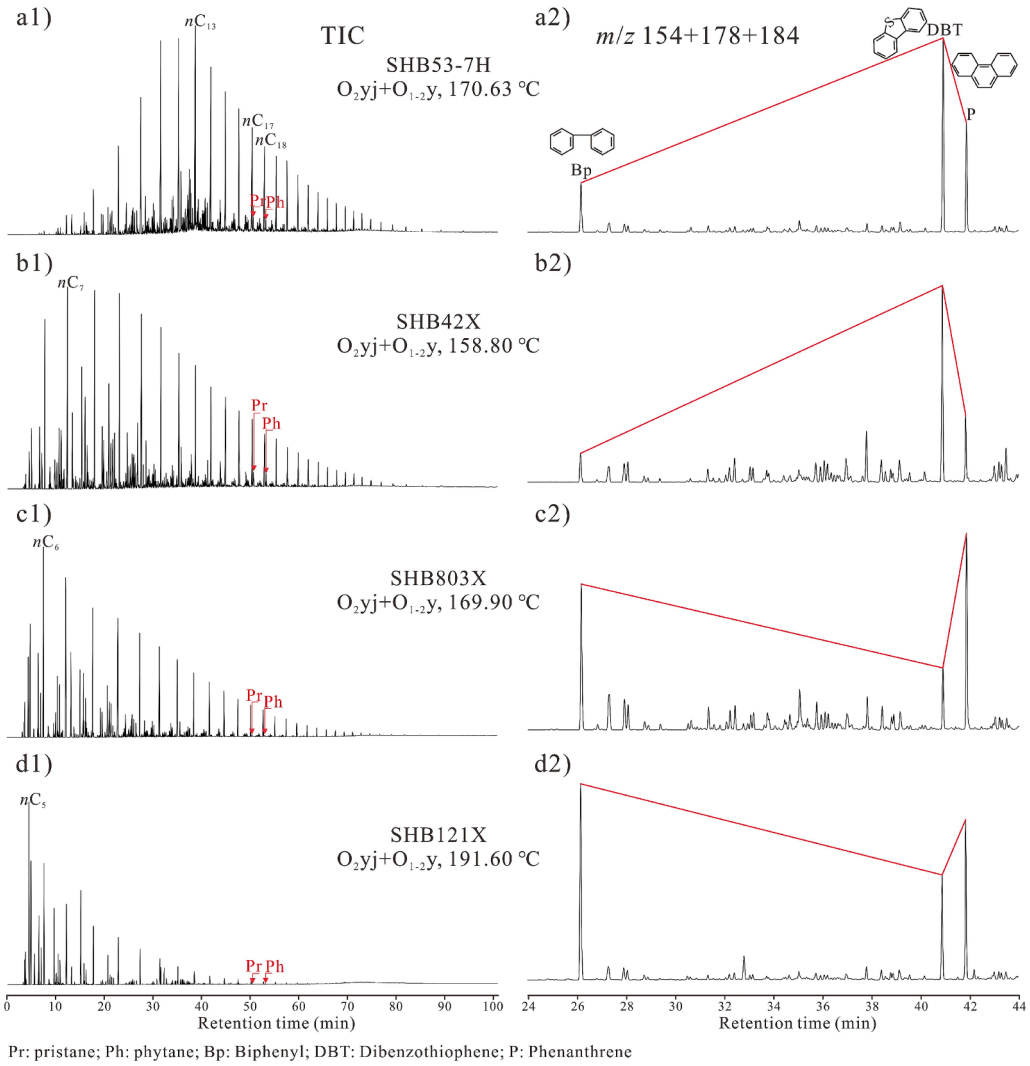

Fig. 2. Representative TIC (a1–d1) and *m/z* (154+178+184) mass chromatograms (a2–d2) in condensates from the Shunbei oilfield.

Table 1
Basic information, saturated, and aromatic parameters of the Shunbei condensates.

Number	Well	Strate	Depth (m)	Pr/Ph	Pr/nC_{17}	Ph/nC_{18}	K_1	A	B	C	DBTs μg/g
1	SHB55X	$O_2yj + O_{1\text{-}2}y$	8050–8100	1.10	0.21	0.21	1.10	1.51	1.73	1.42	704.9
2	SHB53-2H		7754–8887	1.67	0.07	0.05	1.19	2.50	2.76	2.53	582.3
3	SHB53-7H		7710–8431	1.21	0.12	0.11	1.05	2.33	1.71	1.10	424.4
4	SHB57X		7315–7950	1.35	0.05	0.04	1.38	1.90	2.92	3.06	314.9
5	SHB42X		7392–7453	1.17	0.24	0.25	1.18	3.46	3.38	3.78	988.1
6	SHB4-13H		7884–7887	1.42	0.16	0.14	1.37	6.43	5.71	7.10	1209.3
7	SHB4-12H		7649–7652	1.28	0.13	0.13	1.21	3.90	3.62	4.11	1711.5
8	SHB4-6H		8093–8095	1.16	0.24	0.24	1.08	1.69	2.27	2.07	448.9
9	SHB4-4H		7526–7592	1.14	0.17	0.17	1.14	1.50	2.06	1.95	506.5
10	SHB6X		7742–8132	0.92	0.22	0.27	1.09	1.29	2.13	1.50	176.6
11	SHB801X		7691–9145	1.51	0.09	0.07	1.16	0.82	1.94	1.14	45.3
12	SHB803X		7661–8110	1.37	0.08	0.08	1.24	1.08	2.18	1.59	31.1
13	SHB804X		7599–8343	1.50	0.07	0.07	1.37	0.68	1.50	1.03	213.7
14	SHB8-3H		7759–8531	1.50	0.10	0.08	1.19	0.56	1.44	0.79	988.1
15	SHB10X		7809–8591	1.80	0.14	0.12	1.23	1.48	4.26	1.91	2.4
16	SHB12X		7126–8121	1.04	0.22	0.24	1.27	2.55	3.76	1.95	29.7
17	SHB121X		7527–8287	0.99	0.12	0.16	1.30	2.03	1.56	1.11	179.2
18	SHB122X		7290–8520	1.16	0.19	0.20	1.32	2.11	2.97	1.72	108.2

K_1 = (2-MH+2,3-DMP)/ (3-MH+2,4-DMP) (Mango, 1997); A: (Bp+DBT)/P; B: (3-MBp+4-MDBT)/3+1-MP; C: (4-MBp+3+2-MDBT)/2-MP; MH: methylhexane; DMP: dimethylpentane; DBTs: the concentration of total DBT series compounds; P: phenanthrene; Bp: biphenyl; DBT: dibenzothiophene; MP: methylphenanthrenes; MBp: methylbiphenyls; MDBT: methyldibenzothiophene.

Table 2
Thiadiamondoid and Diamondoid parameters of the Shunbei condensates.

Number	DMD/DMA	MD/MA	Rc %	EC_1 %	EC_2	TAs %	TDs	TTs	LDs μg/g	HDs	TeAs	PAs	HAs	1+2- MA	3+4- MD	As	Ds	TAs	T
1	0.20	0.33	1.51	89.32	81.82	84.78	11.54	3.68	5229.79	24.75	21.97	2.78	0.00	643.30	187.22	4189.25	799.68	34.77	41.01
2	0.13	0.20	1.60	94.81	88.63	–	–	–	14831.64	46.23	41.63	4.45	0.15	2442.96	385.30	12757.31	1655.10	4.22	5.32
3	0.12	0.19	1.58	95.12	89.01	81.15	15.71	3.14	17018.74	34.00	30.93	2.93	0.14	3106.71	409.73	14746.30	1924.65	104.83	129.18
4	0.11	0.13	1.59	86.41	78.21	93.55	5.93	0.52	6701.97	25.46	23.79	1.60	0.07	1456.82	147.12	5985.42	579.81	39.41	42.13
5	0.10	0.14	1.51	71.72	59.99	88.47	9.67	1.86	3834.96	50.83	40.31	10.34	0.18	634.15	70.71	3085.61	295.22	41.49	44.91
6	0.09	0.13	1.54	83.65	74.79	83.33	13.86	2.81	7469.77	103.46	75.47	27.38	0.61	1238.59	122.29	6046.68	524.78	177.02	212.43
7	0.10	0.14	1.52	80.82	71.28	83.50	13.25	3.25	5733.55	68.26	50.83	17.10	0.33	955.82	104.26	4816.71	446.69	22.35	26.77
8	0.10	0.14	1.49	63.15	49.36	–	–	–	3216.56	25.22	20.85	4.21	0.16	456.00	54.27	2507.77	232.97	0.14	0.15
9	0.10	0.14	1.51	78.24	68.09	–	–	–	5105.28	36.78	33.62	3.05	0.11	800.11	91.93	4324.29	410.93	2.03	2.75
10	0.10	0.14	1.51	59.85	45.28	–	–	–	3018.54	29.45	27.38	2.04	0.03	432.37	49.82	2342.93	217.24	0.19	0.22
11	0.13	0.17	1.62	93.70	87.25	–	–	–	14419.06	11.92	10.62	1.28	0.02	2273.34	317.41	12833.42	1410.79	0.75	1.25
12	0.11	0.13	1.57	86.53	78.37	–	–	–	8335.85	8.06	7.18	0.87	0.01	1289.10	148.50	7569.19	664.12	0.00	0.00
13	0.12	0.18	1.84	97.32	91.74	–	–	–	26860.72	17.10	16.77	0.31	0.02	5102.66	746.35	23694.05	2873.69	8.73	14.45
14	0.12	0.15	1.61	87.64	79.74	–	–	–	7792.82	8.86	7.93	0.91	0.01	1319.81	161.79	6964.51	717.15	0.00	0.00
15	0.04	0.05	1.61	64.70	51.29	–	–	–	7330.35	35.41	35.41	0.00	0.00	1230.67	56.66	7055.76	253.35	0.09	0.14
16	0.14	0.18	1.91	98.50	93.20	–	–	–	47348.66	28.20	28.20	0.00	0.00	9069.92	1330.26	41494.59	5446.64	1.03	3.47
17	0.12	0.16	1.76	98.48	93.18	–	–	–	57265.66	26.91	25.38	1.53	0.00	9818.06	1313.46	51341.59	5604.05	1.73	4.32
18	0.11	0.14	1.85	98.68	93.43	–	–	–	78902.74	28.97	24.77	4.20	0.00	12609.64	1511.43	71781.32	6691.71	0.15	0.99

DMD: Dimethyldiamantane; DMA: Dimethyladamantane; MD: Methyldiamantane; MA: Methyladamantane; TAs: Thiaadamantanes; TDs: Thiaadiamantanes; TTs: Thiatriamantanes; LDs: Lower diamondoids; HDs: Higher diamondoids; TeAs: Tetramantanes; PAs: Pentamantanes; HAs: Hexamantanes; As: Adamantanes; Ds: Diamantanes; Ts: the concentration of total thiadiamondoids; Rc = 0.0243MDI+0.4389; Extent of cracking: EC; $EC_1 = [1 - C_0/C_c] \times 100$; $EC_2 = 1.2402 \times EC_1$-28.952.

an HP-PONA quartz capillary column (60 m × 0.25 mm × 0.25 μm). See Qiao et al. (2024a) for details on the temperature program and experimental procedures. Additionally, known concentrations of d16-diamantine, d8-dibenzothiophene, and d16-diamantine were added to the condensates, aromatic fractions, and OSCs, respectively, as internal standards.

3.3. GC-IRMS

The carbon isotopes of *n*-alkanes were analyzed using an HP 6890 GC-IRMS (GV Instruments, UK). The GC-IRMS was equipped with an HP-5 MS capillary column (30 m × 0.25 mm × 0.25 μm), with helium as the carrier gas. The detailed temperature program: an initial temperature was set at 80 °C, held for 1.5 min, then increased to 130 °C at a rate of 20 °C /min, and subsequently raised to 310 °C at 4 °C /min, where it was held for 15 min. The accuracy of isotope determination was monitored daily using a mixture of *n*-alkanes (*n*-C_{12} to *n*-C_{35}) obtained from Indiana University, with an accuracy deviation of less than 0.3 ‰. Each sample was analyzed in duplicate to ensure repeatability within ± 0.5 ‰, and the average value was recorded as the final result.

3.4. One-dimensional burial-thermal modeling

PetroMod software was used to reconstruct the burial and thermal histories of the SHB42X well in the Shunbei oilfield. Stratigraphic age and burial depth data were provided by SINOPEC Northwest Company (Urumqi). The formation denudation thickness was calculated based on the thickness ratio of adjacent strata and the change ratio of formation thickness using the connected well profile method outlined. The heat flow value reported by Qiao et al. (2024a) was initially adopted, then corrected and adjusted according to the equivalent vitrinite reflectance (calculated according to the bitumen reflectance).

4. Results

4.1. n-alkanes and aromatics

The total ion chromatogram (TIC) of condensates from the Shunbei oilfield does not display obvious baseline humps (Fig. 2 a1–d1). The *n*-alkanes distribution in the condensates was complete, with no obvious loss, showing a single-peak distribution (Fig. 2 a1–d1). From north to south, the predominant peak carbon of the TIC shifted forward, with a distribution range of *n*-C_5 to *n*-C_{13} (Fig. 2 a1–d1). Additionally, the TIC showed a very low abundance of isoprenoid hydrocarbons (e.g., Pr and Ph) in the condensates (Fig. 2 a1–d1).

Quantitative analysis of aromatics showed significant differences in the content of dibenzothiophene series compounds (DBTs) in condensates from the Shunbei oilfield, ranging from 2.44 to 1711.51 μg/g (Table 1). Mass spectrometry (*m/z* 154, 178, and 184) revealed significant differences in the distribution characteristics of biphenyl (Bp), dibenzothiophene (DBT), and phenanthrene (P) in the condensates (Fig. 2 a2–d2). The distribution of these compounds gradually shifts from DBT-dominated to Bp-dominated from north to south (Fig. 2 a2-d2).

4.2. Thiadiamondoids

GC–MS analysis revealed varying amounts of thiadiamondoids in condensates from the Shunbei oilfield, with concentrations ranging from 0 to 212.43 μg/g (Table 2 and Fig. 3). Most condensates contain only small amounts of thiaadamantanes (Fig. 3). Only six condensates, located in the No. 5 (F5) and No. 4 (F4) fault zones near the Tazhong No. 1 fault zone, exhibit high concentrations of thiadiamondoids, with total concentrations exceeding 20 μg/g (Fig. 1b and Table 2). Additionally, information on the thiadiamondoids studied is provided in Supplementary Table S1. The identification and assignment of

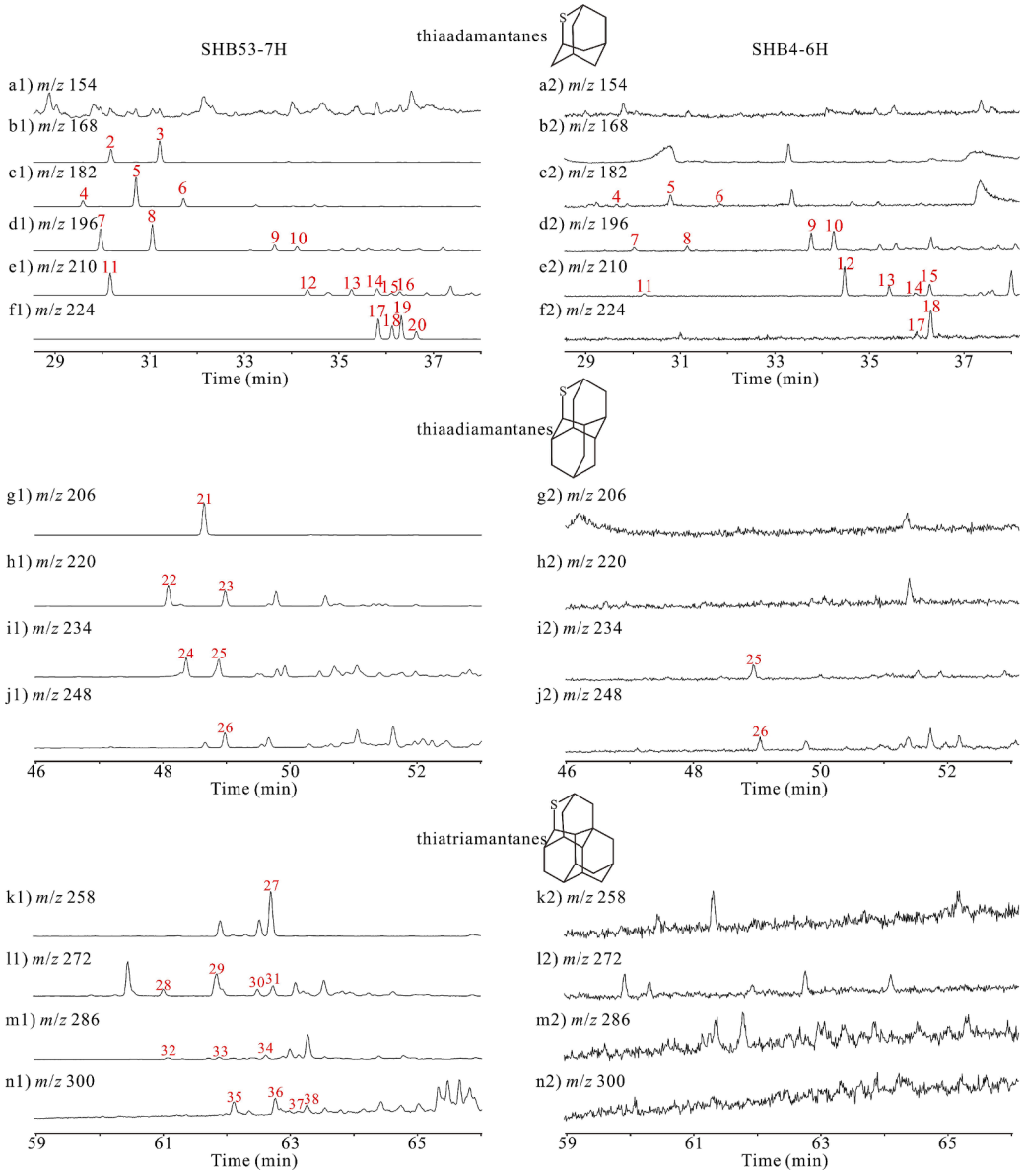

Fig. 3. Mass chromatograms show the distribution of thiadiamondoids in condensate from wells SHB53-7H (a1–n1) and SHB4-6H (a2–n2). Peak labels are listed in Supplementary Table S1.

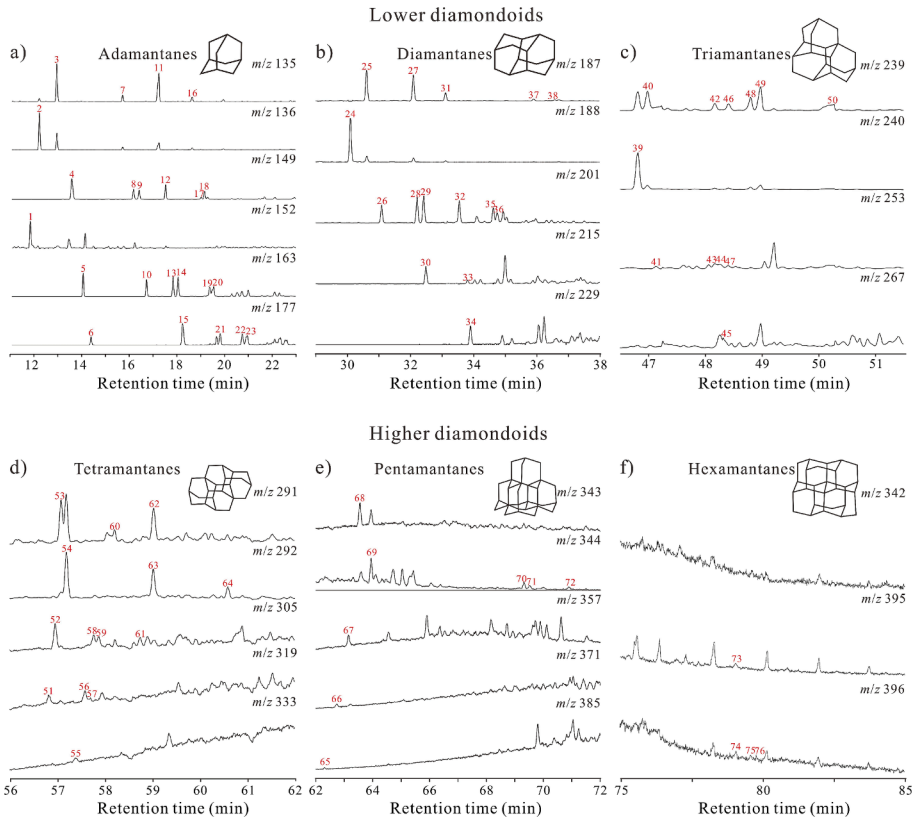

Fig. 4. Mass chromatograms show the distribution of diamondoids in condensate from well SHB53-7H. Peak labels are listed in Supplementary Table S2.

thiadiamondoids referred to Wei et al. (2007, 2011).

4.3. Diamondoids

Supplementary Table S2 presents relevant information on diamondoids in this study, including assignment, abbreviation, molecular formula, and base peak. The identification of diamondoids was based on Wang et al. (2024a,b). The mass chromatogram of diamondoids identified up to 76 compounds in the condensate, including hexamantanes (Fig. 4). Quantitative analysis of the condensates found them rich in diamondoid compounds, with all 18 samples containing significant amounts (Table 2). Lower diamondoids are more prevalent, while higher diamondoids are generally low in concentration. The analysis indicated that diamondoid concentrations decreased exponentially with an increasing number of cages.

4.4. Carbon isotope composition of n-alkane

Carbon isotopes of *n*-alkanes (n-C_{12}–n-C_{34}) from oils in the Shunbei oilfield range from −35.9 ‰ to −26.6 ‰, displaying a wide distribution range (Table 3). Fluctuations in *n*-alkane carbon isotopes across different carbon numbers are minor in most oils, with only a few oils exhibiting significant variations (Table 3).

5. Discussion

5.1. Complex geochemistry and secondary alteration

Over the past two decades, the complex Paleozoic petroleum geochemical properties of the Tarim Basin have drawn significant scholarly attention (Cai et al., 2001; Li et al., 2012; Chen et al., 2018; Bian et al., 2023; Qiao et al., 2024a). Early studies attributed the variations in petroleum geochemical characteristics in the Tarim Basin mainly to oil sources (Li et al., 2010b; Cai et al., 2009a; Chen et al., 2021). Recent petroleum explorations, supported by strong evidence (e.g., sulfur isotopes and aryl isoprenoids), have increasingly recognized the Cambrian Yuertusi Formation ($\epsilon_1 y$) mudstone as the main source rock in the Tarim Basin (Cai et al., 2009b; He et al., 2023). Subsequent studies indicate that petroleum in the Tarim Basin has undergone varying degrees of thermal evolution and diverse secondary processes (e.g., biodegradation, cracking, TSR, evaporative fractionation, and thermal alteration), leading to the observed differences in present geochemical characteristics (Cai et al., 2001; Zhang et al., 2011).

The exploration depth of the Shunbei oilfield ranges from 7000 to 10,000 m. Since the initial oil charge during the late Caledonian, the reservoir's oil has been influenced by various factors, including structural adjustment, microorganisms, hydrothermal activity, and formation temperature. Qiao et al. (2024a) detected 25-norhopane series compounds in the oil, indicating biodegradation. Late gas charging has led to significant evaporative fractionation, as indicated by the distribution of *n*-alkane molar concentrations and light hydrocarbon parameters (e.g., Tol/nC$_7$ and nC$_7$/MCH) (Qiao et al., 2024a). The TIC of the condensates in this study also displayed varying degrees of *n*-alkane fractionation (Fig. 2 a1–d1).

Previous studies on the extent of cracking (EC) in condensates from the Shunbei oilfield were mainly characterized by the 3-+4-methyldiamantane (3-+4-MD) concentrations, revealing significant variations in the EC (Bian et al., 2023; Qiao et al., 2024a). Diamondoid concentrations in oils may be influenced by evaporative fractionation and TSR; consequently, the applicability of 3-+4-MD concentrations in condensates from the Shunbei oilfield to characterize the EC needs to be considered (see Section 5.2).

Previous studies indicate a hydrothermal upwelling event in the Tarim Basin during the Permian (Cai et al., 2008; Guo et al., 2016; Li et al., 2022). Xu et al. (2022) confirmed that the oils in the Shunbei oilfield were affected by hydrothermal alteration through the

Table 3
The carbon isotopic compositions of *n*-alkanes of oils from the Shunbei oilfield.

Well	$\delta^{13}C_{PDB}$, ‰																						
	nC_{12}	*n*C_{13}	*n*C_{14}	*n*C_{15}	*n*C_{16}	*n*C_{17}	*n*C_{18}	*n*C_{19}	*n*C_{20}	*n*C_{21}	*n*C_{22}	*n*C_{23}	*n*C_{24}	*n*C_{25}	*n*C_{26}	*n*C_{27}	*n*C_{28}	*n*C_{29}	*n*C_{30}	*n*C_{31}	*n*C_{32}	*n*C_{33}	*n*C_{34}
SHB4-13H	–	−30.7	−31.0	−31.1	−31.4	−31.5	−31.7	−32.0	−32.0	−32.1	−32.2	−32.2	−32.3	−32.3	−32.4	−32.3	−32.3	−32.5	−32.6	−32.5	−32.5	−32.3	
SHB4-4H	–	–	−34.4	−34.4	−34.5	−34.2	−34.2	−34.0	−33.9	−34.1	−33.9	−34.3	−34.0	−34.2	−34.2	−34.1	−34.2	−34.2	−34.4	−34.5	−34.1	−34.2	−34.4
SHB42X	−32.8	−33.1	−33.2	−33.1	−33.5	−33.5	−33.6	−33.4	−33.4	−33.4	−33.5	−33.4	−33.6	−33.7	−33.8	−33.9	−33.4	−33.7	−33.1	−33.1	–	–	–
SHB6X	−33.2	−33.1	−33.1	−33.2	−33.3	−33.3	−33.4	−33.5	−33.4	−33.5	−33.5	−33.5	−33.5	−33.5	−33.5	−33.5	−33.5	−33.7	−33.7	−33.8	−33.6	−34.0	−33.8
SHB82X	–	−31.6	−31.6	−31.7	−31.9	−32.0	−32.1	−32.1	−32.2	−32.2	−32.2	−32.3	−32.3	−32.4	−32.4	−32.3	−32.7	−32.6	−32.7	−32.8	−32.3	–	–
SHB804X	–	–	−28.6	−28.6	−29.3	−29.3	−29.1	−29.1	−29.3	−29.4	−29.4	−29.7	−30.1	−29.7	−29.2	−30.0	−28.3	–	–	–	–	–	–
SHB10X	–	−32.1	−32.1	−32.2	−32.0	−32.3	−32.6	−32.1	−32.5	−31.4	−31.2	−32.9	–	–	–	–	–	–	–	–	–	–	–
SHB12X	−33.4	−33.3	−33.1	−33.2	−33.3	−33.3	−33.1	−33.2	−33.2	−33.1	−33.1	−32.9	−32.6	−32.5	−32.5	−32.3	–	−29.5	−29.6	–	–	–	–
SHB121X	−26.6	−26.8	−27.2	−27.5	−28.1	−28.4	−28.5	−29.1	−29.3	−29.6	−29.6	−29.4	−29.7	−30.0	−29.7	−29.6	−29.5	−29.9	−28.9	–	–	–	–
SHB122X	−31.6	−31.9	−31.9	−32.1	−32.0	−32.0	−31.9	−32.0	−32.0	−31.9	−31.9	−31.7	−31.4	−31.3	−31.1	−30.9	−30.9	−31.1	−31.4	−30.6	−31.2	–	–
SHB53-7H[a]	–	–	−34.1	−34.3	−34.5	−34.3	−34.1	−34.4	−35.8	−35.2	−35.2	−35.8	−35.1	−35.6	−35.2	−35.1	−35.9	–	–	–	–	–	–
SHB53-2H[a]	–	–	−31.8	−32.0	−32.8	−32.1	−32.0	−33.3	−32.8	−33.1	−33.1	−33.1	−32.5	−32.7	−32.4	−32.9	−32.9	−32.1	–	–	–	–	–
SHB55X[a]	–	–	−32.5	−33.5	−33.9	−33.2	−34.4	−33.9	−33.9	−33.8	−34.3	−34.5	−33.8	−34.3	–	–	–	–	–	–	–	–	–
SHB57X[a]	–	–	−27.5	−28.9	−28.5	−29.3	−30.6	−28.9	−29.3	−29.3	−30.5	−29.6	−29.7	−30.1	−29.8	−30.7	−30.4	–	–	–	–	–	–

[a] From Qiao et al. (2024a); "–": no data or not determined.

conversion of "P-Bp-DBT" series compounds. H^+ and S^+ carried during hydrothermal upwelling promote the conversion of P series compounds to DBT and Bp series compounds (Xu et al., 2022; Xu et al., 2024). In addition, the Ordovician reservoir of the Shunbei oilfield has also provided additional strong evidence of hydrothermal alteration, including the high content of >5-ring PAHs in oil (Qiao et al., 2024a), high homogenization temperature (Xu et al., 2022), positive Eu anomaly (Li et al., 2023), and strontium isotope compositions (Li et al., 2023).

In this study, mass spectrometry (*m/z* 154, 178, and 184) showed significant differences in the distribution characteristics of Bp, DBT, and P in condensates (Fig. 2 a2–d2). According to the conversion path of "P-Bp-DBT" series compounds proposed by Xu et al. (2022), the ratios (DBT+Bp)/P, (2 + 3-MDBT+4-MBp)/2-MP, and (4-MDBT+3-MBP)/3 + 1-MP were selected as indicators to identify the intensity of hydrothermal alteration in condensates (Fig. 5). The results indicate that the condensate oil in F5 and F4 near the Tazhong No. 1 fault zone experienced more intense hydrothermal alteration (Fig. 5 and Table 1). This indicates that these wells may be closer to hydrothermal upwelling channels.

TSR is an important secondary process in reservoirs involving a series of redox reactions between organic matter and sulfate to generate H_2S, CO_2, sulfur- and oxygen-bearing compounds, and diamondoids with thiols as intermediate products at temperatures > 130 °C (Machel et al., 1995; Cai et al., 2003, 2022). For the Tarim Basin, TSR evidence was first identified in the Tazhong oilfield (Cai et al., 2009b). The light hydrocarbon parameters and quantitative analysis of organic sulfur compounds revealed varying degrees of TSR influence in different areas of the Tazhong oilfield (Cai et al., 2016a, 2016b; Song et al., 2017). Cai et al. (2016a) analyzed organic sulfur compounds and sulfur isotope compositions and concluded that thiadiamondoids were generated *in situ* in the Cambrian and Ordovician formations of the Tazhong oilfield. Additionally, thiadiamondoids generated in the Cambrian contributed to Ordovician reservoirs (e.g., ZG46 and TZ201C) during petroleum charging (Cai et al., 2016a).

Whether condensates in the Ordovician reservoir of the Shunbei oilfield are affected by TSR remains controversial. Wang et al. (2023) concluded that part of the condensates in Ordovician reservoirs of the Shunbei oilfield had been affected by TSR through the detection of thiadiamondoids. However, based on the requirements for the occurrence of TSR, light hydrocarbon parameters, and quantitative analysis of sulfur compounds, most scholars believe that the condensates in the Ordovician reservoir of the Shunbei oilfield have not been affected by TSR. The evidence for TSR is likely due to petroleum that migrated into Ordovician reservoirs along with late gas charging (Qiao et al., 2024a). Building on previous studies, this research further examines whether condensates in the Ordovician reservoir of the Shunbei oilfield have been affected by TSR. Only six condensates, located in the F5 and F4 near the Tazhong No. 1 fault zone, had total thiadiamondoid concentrations exceeding 28 μg/g, potentially indicating TSR (Fig. 6a; Cai et al., 2016a). However, a comparative analysis of the relative percentage contents of thiaadamantanes, thiadiamantanes, and thiatriamantanes in condensates showed that the proportion of thiaadamantanes was significantly higher, ranging from 81.15 % to 93.55 % (Fig. 6b and Table 2). The distribution characteristics of lower thiadiamondoids are significantly different from those of wells ZS1C and ZS5 oils, which are clearly affected by TSR (Zhu et al., 2023). These distributions suggest that TSR occurred in the Ordovician reservoirs at these locations, but the impact of TSR may be limited.

Previous studies have shown that besides generating thiadiamondoid, TSR also increases the K_1 value (Mango, 1997) and DBTs concentration in oil (Orr, 1974). The K_1 value of oil in the Shunbei oilfield exceeds 1.0, suggesting the possible occurrence of TSR in Ordovician reservoirs (Fig. 6c). However, the distribution patterns of 2-MH+2, 3-DMP, and 3-MH+2, 4-DMP differ markedly from those in oil affected by TSR in the Tazhong oilfield. In combination with DBTs concentration analysis, the DBTs concentration in the Shunbei oilfield is

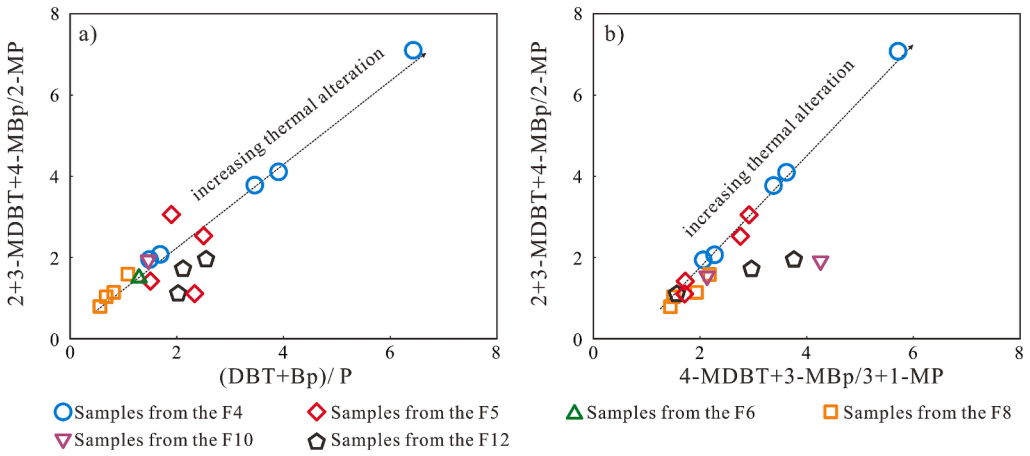

Fig. 5. Cross-plots showing the intensity of hydrothermal alteration in condensates from the Shunbei oilfield (modified after Xu et al., 2022). a) (3+2-MDBT+4-MBp)/2-MP versus (Bp+DBT)/P; b) (3+2-MDBT+4-MBp)/2-MP versus (4-MDBT+3-MBp)/3+1-MP; P: phenanthrene; Bp: biphenyl; DBT: dibenzothiophene; MP: methylphenanthrenes; MBp: methylbiphenyls; MDBT: methyldibenzothiophene.

notably less than 2000 μg/g, which falls within the contribution range of source rocks (Table 1; Cai et al., 2016b). Additionally, the DBTs concentration in the Shunbei oilfield is significantly lower than in the TSR-affected oil from the Tazhong oilfield (Fig. 6d). Further analysis reveals no clear linear correlation between thiadiamondoid and DBTs concentrations in Shunbei oil (Fig. 6e and f; Cai et al., 2016a).

For SHB42X, the TAs concentration is 41.49 μg/g, and the $\delta^{34}S$ values of DBTs range from 19.0 ‰ to 23.4 ‰ (Wang et al., 2024a,b). The $\delta^{34}S$ values are similar to the Cambrian source rock kerogens (14.0 ‰–21.6 ‰) (Cai et al., 2015). The $\delta^{34}S$ values differ significantly from those of Cambrian anhydrites (26.8 ‰–34.1 ‰) and Ordovician anhydrites (26.0 ‰) (Cai et al., 2001; Cai et al., 2016a). This suggests that TSR has not significantly influenced the DBTs in the oil.

Maturity influences carbon isotope fluctuations in *n*-alkanes, typically ranging from 2.0 ‰ to 3.0 ‰, which can effectively record the source information of organic matter (Clayton and Bjorøy, 1994; Chen et al., 2022). Previous studies have shown that TSR and thermal alteration can lead to heavier carbon isotopes in *n*-alkanes (Li et al., 2010b, 2015; Cai et al., 2015). Notably, ZS1C (affected by TSR) and TD2 (affected by thermal alteration) serve as representative samples (Fig. 7). The carbon isotope data of *n*-alkanes in the Shunbei oilfield indicate a more pronounced influence of thermal alteration. For example, the *n*-alkane carbon isotopes of SHB53-7H, SHB42X, and SHB4-13H oils with higher thiadiamondoid concentrations do not exhibit a significant increase (Fig. 7 and Table 3). However, the carbon isotopes in oil with low thiadiamondoid concentrations from SHB121X and SHB804X show a significant enrichment of heavier isotopes (Fig. 7 and Table 3). This further supports the conclusion that TSR has not significantly altered the oil properties in the Ordovician reservoir.

Wang et al. (2024a,b) detected the $\delta^{34}S$ values of VOSCs and H_2S in well SHB44X, which indicated a mixture of VOSCs and H_2S originating from Cambrian TSR. This suggests a hydrothermal upwelling from deep within the basin during the Permian Large Igneous Province (Xu et al., 2022; Li et al., 2023). Hydrothermal activities and local thermal anomalies provide the necessary water environment and temperature for TSR (Fig. 8). Intense TSR occurs in the salt-gypsum reservoirs of the Cambrian Awatage and Shayilike formations. VOSCs, H_2S, and altered oils (containing low thiadiamondoids) entered the Ordovician reservoir during petroleum charging. However, the $\delta^{13}C$ of *n*-alkanes, DBTs concentration, and δ^{34S} values of DBTs from SHB42X oil indicate no significant TSR impact (Fig. 6, Fig. 7; Wang et al., 2024a,b). This suggests that TSR-affected oil either did not charge the Ordovician reservoir or entered in minimal amounts. Additional H_2S and VOSCs entered the Ordovician reservoirs. Under hydrothermal influence, H_2S entering the Ordovician system interacted with hydrocarbons through TSR, forming some thiadiamondoids. However, the limited quantity of H_2S entering the Ordovician reservoir and the constraints of the hydrothermal upwelling channel restricted the extent and impact of TSR. During the late gas charging phase, smaller molecular compounds like VOSCs, H_2S, and TAs from the Cambrian system charged the Ordovician reservoir, supplementing the TSR evidence. A comprehensive analysis indicates that neither Cambrian nor Ordovician TSR significantly affected DBTs in current Ordovician oil.

5.2. Stability of diamondoid parameters

The condensates in the Shunbei oilfield have undergone multiple secondary alterations. Among these, partial alteration, such as evaporative fractionation, significantly affects diamondoids in oil (Moldowan et al., 2015). The strong evaporative fractionation can lead to unequal ratios of adamantanes (As) and diamantanes (Ds), altering their ratio in oils (Moldowan et al., 2015). By comparing 1-+2-methyladamantane (1-+2-MA) and 4-+3-MD in the Shunbei oilfield condensates, a strong linear relationship was observed, $R^2 = 0.9807$ (Fig. 9a). Similarly, As and Ds also showed a strong linear relationship, $R^2 = 0.9631$ (Fig. 9b). This indicates that diamondoids (especially Ds) in the Shunbei oilfield are minimally or not affected by evaporative fractionation (Fig. 9). In addition, previous simulation experiments have found that MDI shows a slight floating change in the process of evaporation fractionation, which can still effectively indicate the maturity of oil (Li et al., 2014; Qiao et al., 2024b).

Diamondoids have strong biodegradation resistance (Grice et al., 2000). However, at a PM biodegradation level above 6, diamondoids begin to degrade (Song et al., 2024). The presence of complete 25-norhopane series compounds in the Shunbei oilfield condensates indicates a PM biodegradation level above 6 (Qiao et al., 2024a). The biodegradation resistance of diamondoids depends on the number of cages, alkylation degree, and substituent positions (Cheng et al., 2018). Among these, As is more susceptible to biodegradation than Ds at PM levels above 6 (Song et al., 2024). Analyses of As/Ds, MD/MA, and DMD/DMA ratios effectively indicate biodegradation intensity (Fig. 10). Fig. 10 shows that MD/MA versus DMD/DMA and As/Ds versus DMD/DMA cross-plots are consistent in the identification of biodegradation degree, indicating that biodegradation has not significantly affected Ds in the Shunbei oilfield condensates.

Besides evaporative fractionation and biodegradation, TSR significantly affects diamondoids (Peng et al., 2022). The detection of thiadiamondoids shows that their total concentrations in some condensates in the Shunbei oilfield exceed 28 μg/g, with thiaadamantanes being the main component (Table 2). Comprehensive analysis reveals that TSR did

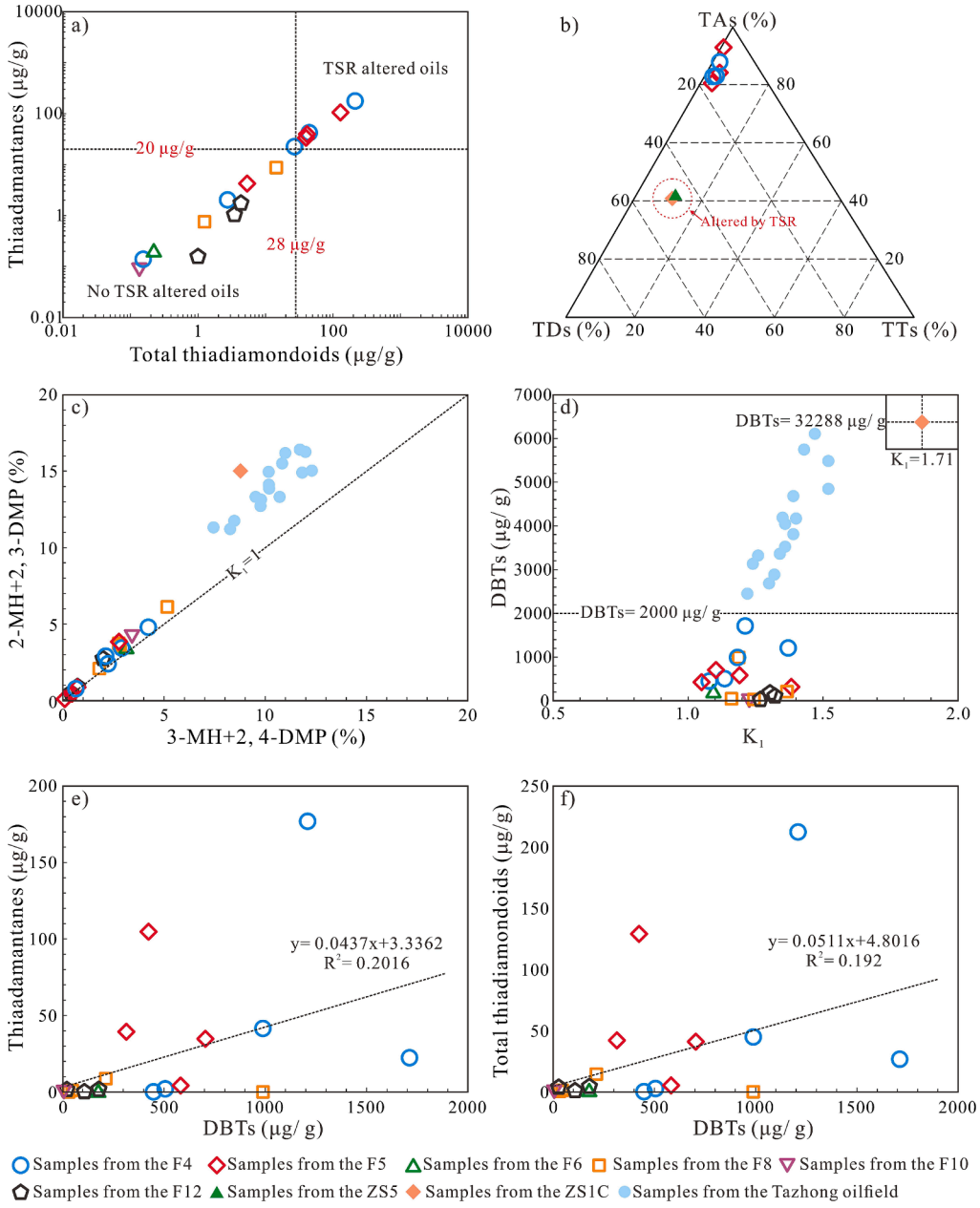

Fig. 6. A cross-plot and ternary diagram identify the thermochemical sulfate reduction in condensates from the Shunbei oilfield. a) TAs concentrations versus Ts concentrations (TAs threshold values from Cai et al. (2016b), Ts threshold values from Cai et al. (2016a)); b) ternary diagram of TAs, TDs, and TTs (data for ZS5 and ZS1C are from Zhu et al. (2023)); c) 3-MH+2,4-DMP (%) versus 2-MH+2,3-DMP (%) (Tazhong data from Song et al. (2017)); d) K_1 versus DBTs concentrations (Tazhong data from Song et al. (2017)); e) TAs concentrations versus DBTs concentrations; f) Ts concentrations versus DBTs concentrations; TAs: total thiadiamondoids; TAs: thiaadamantanes; TDs: thiaadiamantanes; TTs: thiatriamantanes.

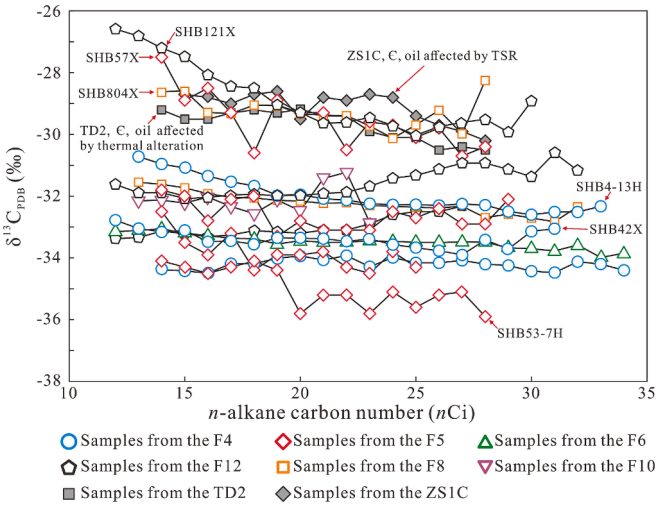

Fig. 7. Cross-plots of carbon number and carbon isotope compositions of n-alkane patterns of oils from the Shunbei oilfield. Comparative data for F5 oil is from Qiao et al. (2024a), ZS1C oil data is from Li et al. (2015), and TD2 oil data is from Li et al. (2010a).

not occur in the Ordovician reservoir. Instead, the abundant thiadiamondoids were introduced with late gas charging. Therefore, there is no TSR influence affecting diamondoids in the condensates in the Shunbei oilfield.

Based on the above analysis, we conclude that the diamondoids in the condensates of the Shunbei oilfield are either unaffected by complex secondary processes or are only slightly affected; hence, diamondoids can be used effectively to chacterize their maturity and EC. The calculated vitrinite reflectance (R_c) using MDI (R_c = 0.0243 MDI+0.4389) ranges from 1.49 % to 1.90 % (Table 2; Chen et al., 1996), consistent with the condensates at a high maturity stage. Based on the stability of diamondoids, the EC_1 ($EC_1 = [1\text{-}C_0/C_c] \times 100$) in the condensates was quantified using the concentrations of 3-+4-MD (Dahl et al., 1999). The baseline concentration of 3-+4-MD was set at 20 μg/g, based on previous studies (Qiao et al., 2024a). EC_1 of the condensates from the Shunbei oilfield ranges from 59.85 % to 98.68 % (Table 2). Considering the effect of newly generated diamondoids, the correction formula of Peng et al. (2022) ($EC_2 = 1.2402 \times EC_1\text{-}28.952$) was adopted for further calculation. The distribution of EC_2 ranged from 45.28 % to 93.43 %. The EC_2 in the condensates of the Shunbei oilfield varies significantly and is distributed across all stages of cracking.

5.3. Origin of higher diamondoids

Early studies on diamondoids as hydrocarbon compounds with high thermal stability mostly focused on the series parameters of adamantanes, diamantanes, and their derivatives (Dahl et al., 1999; Moldowan et al., 2015). This focus is mainly due to the detection of triamantanes and higher diamondoids in a small fraction of oils undergoing high thermal evolution (Cai et al., 2016a). Simulation experiments suggested a close relationship between the formation of higher diamondoids and the degree of thermal evolution (Wei et al., 2007). However, this view may have limitations due to the restricted study sample.

The origin of higher diamondoids in 18 condensates from the Shunbei oilfield was analyzed. Pearson correlation was used to create a heat map for the relevant parameters, including diamondoid and thiadiamondoid concentrations, sedimentary environment, maturity, EC, evaporative fractionation, biodegradation, TSR, and hydrothermal alteration (Fig. 11). The results showed a significant positive correlation among higher diamondoids (R^2 ranging from 0.86 to 0.99). However, no significant correlation exists between higher and lower diamondoids in the Shunbei oilfield condensates (R^2 ranging from −0.32 to −0.14). Additionally, Fig. 11 shows that higher diamondoid concentrations do not significantly correlate with the sedimentary environment, maturity, EC, evaporative fractionation, or biodegradation. This indicates no genetic relationship between higher diamondoids in the Shunbei oilfield condensates and these factors. Specifically, the correlation coefficient between higher diamondoid concentrations and condensate maturity was low (R^2 ranging from −0.41 to −0.25). This suggests that the origin of higher diamondoids in Shunbei oilfield condensates is unrelated to thermal evolution and may have a unique genetic mechanism.

Higher diamondoid, thiadiamondoid, and DBTs concentrations were positively correlated with the hydrothermal parameters. The correlation coefficient between thiadiamondoids and hydrothermal parameters ranges from 0.50 to 0.76 suggesting that the formation of thiadiamondoids is related to hydrothermal activity. Higher diamondoids did not have the potential to migrate into present-day Ordovician reservoirs suggesting that hydrothermal activity may have led to the formation of higher diamondoids in the Shunbei oilfield. Local thermal anomalies during hydrothermal activity meet the temperature requirements for the formation of higher diamondoids (Wei et al., 2007; Li et al., 2022). Additionally, H^+ produced by the reaction of water with organic compounds can promote compound conversion (Schimmelmann et al., 1999; Xu et al., 2022). This is consistent with early thermal simulation experiments, which indicate that water promotes the formation of higher diamondoids (Wei et al., 2007; Fang et al., 2013), which is supported by a positive correlation (R^2 ranging from 0.59 to 0.76) between higher diamondoids and the hydrothermal origin of DBTs. In addition, higher diamondoids exhibit a significant positive correlation with parameters indicating the intensity of hydrothermal activity (R^2 ranging from 0.67 to 0.95). In summary, higher diamondoids in the Shunbei oilfield condensates are believed to have formed by hydrothermal activities rather than normal thermal evolution.

Previous simulation experiments show that the four oil fractions can be pyrolyzed to form diamondoids (Fang et al., 2013). Peng et al. (2022) conducted a simulation experiment with conditions similar to the hydrothermal environment in the Tarim Basin and showed that diamondoids were formed (Fig. 12). The Shunbei oilfield condensates are at a high stage of thermal evolution and are rich in lower diamondoid concentrations (Table 2). Furthermore, since hydrothermal activity is transient, the lower diamondoids formed through this pathway constitute a minor portion of the overall lower diamondoid content in the condensates and likely can be disregarded.

6. Conclusions

Supporting previous studies, diamondoids in the Shunbei oilfield

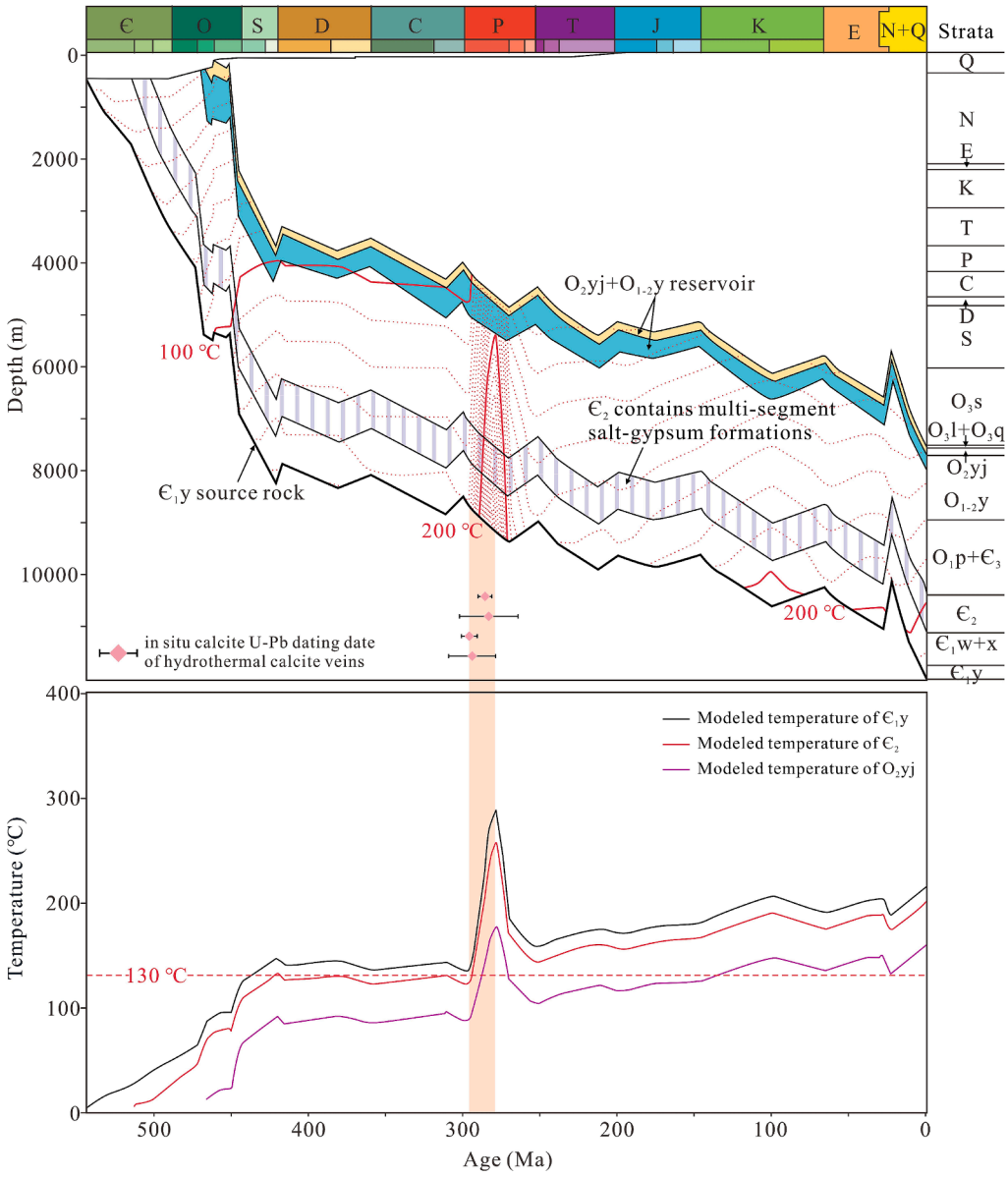

Fig. 8. Burial-thermal history and reservoir temperature evolution of well SHB42X. In situ calcite U-Pb dating date of hydrothermal calcite veins from Li et al. (2023).

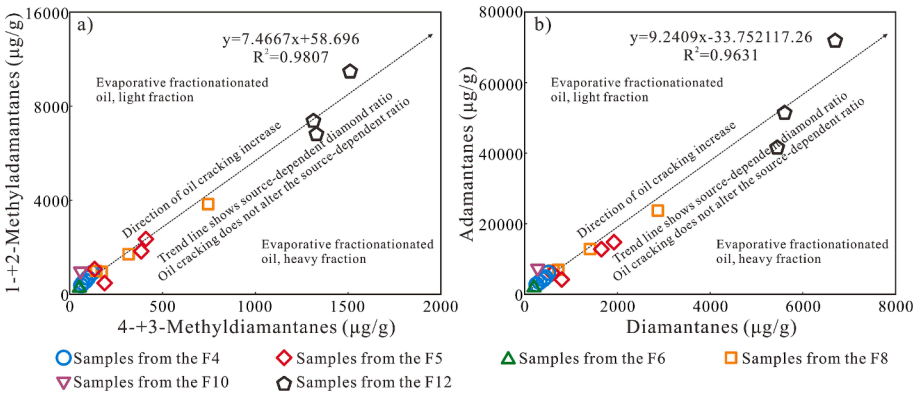

Fig. 9. Cross-plots showing the intensity of evaporative fractionation in condensates from the Shunbei oilfield (refer to Moldowan et al., 2015). a) 1-+2-methyladamantane concentrations versus 4-+3-methyldiamantane concentrations; b) Adamantanes concentrations versus diamantanes concentrations.

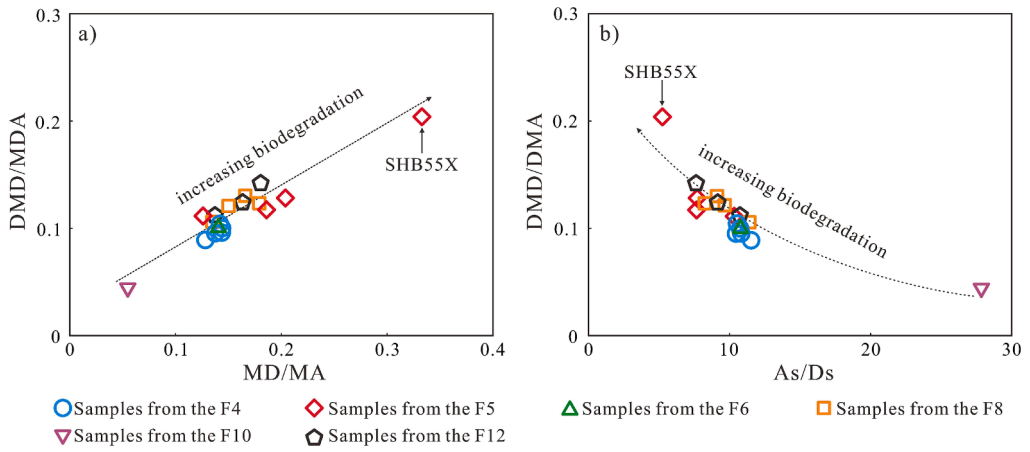

Fig. 10. Cross-plots showing the intensity of biodegradation in condensates from the Shunbei oilfield (refer to Song et al., 2024). a) DMD/DMA versus MD/MA; b) DMD/DMA versus As/Ds; DMD: Dimethyldiamantane; DMA: Dimethyladamantane; MD: Methyldiamantane; MA: Methyladamantane; As: Adamantanes; Ds: Diamantanes.

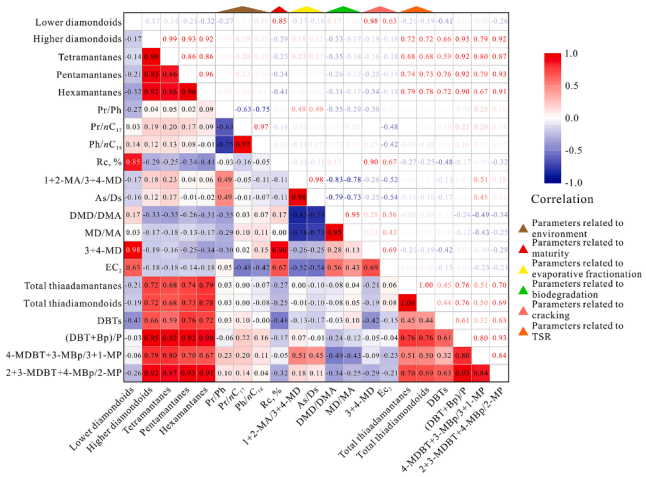

Fig. 11. The correlation heat map of diamondoid concentrations with depositional environment parameters, maturity parameters, evaporative fractionation parameters, biodegradation parameters, extent of cracking parameters, thiadiamondoid concentrations, and hydrothermal alteration parameters.

condensates indicate that these samples have undergone multiple secondary alterations. High local concentrations of thiaadamantanes in oil may result from the interaction of H_2S, derived from Cambrian TSR, with Ordovician hydrocarbons, influenced by hydrothermal activities. Comprehensive analysis shows that TSR is local and limited in Ordovician reservoirs in Shunbei oilfield and has no significant impact on oil.

The distribution characteristics of 1-+2-MA/3-+4-MD, As/Ds, MD/MA, and DMD/DMA indicate that biodegradation and evaporation fractionation have no significant effect on diamondoids in the Shunbei oilfield condensates. Specifically, the parameters related to diamantane compounds in the condensates effectively characterize their geochemical properties and secondary alterations.

The "P-Bp-DBT" series compounds indicate significant hydrothermal alteration in the Shunbei oilfield condensates. The origin of higher diamondoids in the condensates was analyzed using a correlation heat map of parameters such as diamondoid and thiadiamondoid concentrations, sedimentary environment, maturity, EC, evaporative fractionation, biodegradation, TSR, and hydrothermal alteration. The result suggests that the origin of higher diamondoids in Shunbei oilfield condensates is unrelated to thermal evolution and may have a unique genetic mechanism.

This study revealed a formation pathway of higher diamondoids under hydrothermal activity. This unique thermal evolution of higher diamondoids offers a new perspective on hydrothermal activity in organic geochemistry. Furthermore, this helps in examining the organic–inorganic interactions of ultra-deep organic fluids with their mineralogical and aqueous environments.

CRediT authorship contribution statement

Rongzhen Qiao: Writing – review & editing, Writing – original draft, Visualization, Methodology, Investigation. **Meijun Li:** Writing – review & editing, Visualization. **Donglin Zhang:** Software, Investigation, Data curation. **Hong Xiao:** Supervision.

Declaration of competing interest

The authors declare that they have no known competing financial interests or personal relationships that could have appeared to influence the work reported in this paper.

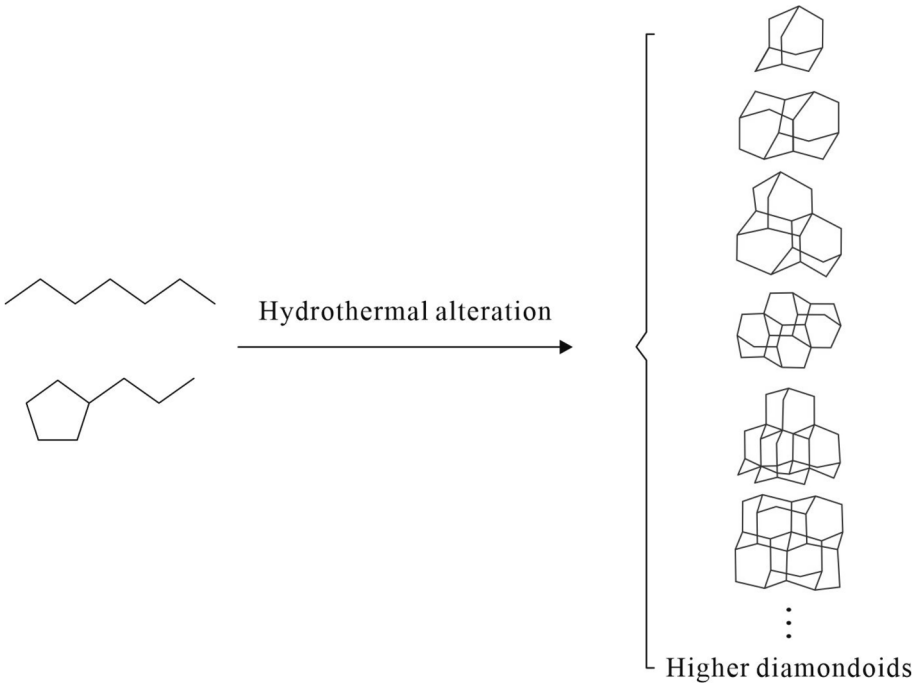

Fig. 12. Possible pathways for the formation of diamondoids under the influence of hydrothermal activity (modified after Peng et al., 2022).

Data availability

Data will be made available on request.

Acknowledgements

This work was funded by the National Natural Science Foundation of China (Grant No. 42173054). The author expresses gratitude to the Editor-in-Chief, Clifford C. Walters, Executive Guest Editor, Huiyuan (Ian) Xu, and the two anonymous reviewers for their valuable and constructive reviews, which have significantly enhanced the manuscript.

Appendix A. Supplementary data

Supplementary data to this article can be found online at https://doi.org/10.1016/j.orggeochem.2024.104883.

References

Atwah, I., Moldowan, J.M., Koskella, D., Dahl, J., 2021. Application of higher diamondoids in hydrocarbon mudrock systems. Fuel 284, 118994.
Berwick, L., Alexander, R., Pierce, K., 2011. Formation and reactions of alkyl adamantanes in sediments: carbon surface reactions. Organic Geochemistry 42, 752–761.
Bian, J., Hou, D., Cui, Y., Zhu, X., 2023. Geochemical characteristics and origin of the ultra-deep hydrocarbons from the Shunbei Oilfield in the Tarim Basin, China: insight from molecular biomarkers and carbon isotope geochemistry. Marine and Petroleum Geology 158, 106542.
Cai, C., Hu, W., Worden, R.H., 2001. Thermochemical sulphate reduction in Cambro-Ordovician carbonates in Central Tarim. Marine and Petroleum Geology 18, 729–741.
Cai, C., Worden, R.H., Bottrell, S.H., Wang, L., Yang, C., 2003. Thermochemical sulphate reduction and the generation of hydrogen sulphide and thiols (mercaptans) in Triassic carbonate reservoirs from the Sichuan Basin, China. Chemical Geology 202, 39–57.
Cai, C., Li, K., Li, H., Zhang, B., 2008. Evidence for cross formational hot brine flow from integrated $^{87}Sr/^{86}Sr$, REE and fluid inclusions of the Ordovician veins in Central Tarim, China. Applied Geochemistry 23, 2226–2235.
Cai, C., Li, K., Ma, A., Zhang, C., Worden, R.H., Xu, Z., Wu, G., Zhang, B., Chen, L., 2009a. Distinguishing the Cambrian source rock from the Upper Ordovician: evidence from sulfur isotopes and biomarkers in the Tarim Basin. Organic Geochemistry 40, 755–768.
Cai, C., Zhang, C., Cai, L., Wu, G., Jiang, L., Xu, Z., Li, K., Ma, A., Chen, L., 2009b. Origins of Palaeozoic oils in the Tarim Basin: evidence from sulfur isotopes and biomarkers. Chemical Geology 268, 197–210.
Cai, C., Zhang, C., Worden, R.H., Wang, T., Li, H., Jiang, L., Huang, S., Zhang, B., 2015. Application of sulfur and carbon isotopes to oil–source rock correlation: a case study from the Tazhong area, Tarim Basin, China. Organic Geochemistry 83–84, 140–152.
Cai, C., Xiao, Q., Fang, C., Wang, T., He, W., Li, H., 2016a. The effect of thermochemical sulfate reduction on formation and isomerization of thiadiamondoids and diamondoids in the Lower Paleozoic petroleum pools of the Tarim Basin, NW China. Organic Geochemistry 101, 49–62.
Cai, C., Amrani, A., Worden, R.H., Xiao, Q., Wang, T., Gvirtzman, Z., Li, H., Said-Ahmad, W., Jia, L., 2016b. Sulfur isotopic compositions of individual organosulfur compounds and their genetic links in the Lower Paleozoic petroleum pools of the Tarim Basin, NW China. Geochimica et Cosmochimica Acta 182, 88–108.
Cai, C., Li, H., Li, K., Wang, D., 2022. Thermochemical sulfate reduction in sedimentary basins and beyond: a review. Chemical Geology 607, 121018.
Chen, Z., Wang, T.-G., Li, M., Yang, F., Cheng, B., 2018. Biomarker geochemistry of crude oils and Lower Paleozoic source rocks in the Tarim Basin, western China: an oil-source rock correlation study. Marine and Petroleum Geology 96, 94–112.
Chen, Z., Chai, Z., Cheng, B., Liu, H., Cao, Y., Cao, Z., Qu, J., 2021. Geochemistry of high-maturity crude oil and gas from deep reservoirs and their geological significance: a case study on Shuntuoguole low uplift, Tarim Basin, western China. AAPG Bulletin 105, 65–107.
Chen, J., Fu, J., Sheng, G., Liu, D., Zhang, J., 1996. Diamondoid hydrocarbon ratios: novel maturity indices for highly mature crude oil. Organic Geochemistry 25, 179–190.
Chen, Z., Qiao, R., Li, C., Wang, D., Gao, Y., 2022. Hydrocarbon generation potential and model of the deep lacustrine source rocks in the Dongying Depression, Bohai Bay Basin. Marine and Petroleum Geology 140, 105656.
Cheng, X., Hou, D.J., Xu, C.G., 2018. The effect of biodegradation on adamantanes in reservoired crude oils from the Bohai Bay Basin, China. Organic Geochemistry 123, 38–43.
Clayton, C.J., Bjorøy, M., 1994. Effect of maturity on ^{13}C ^{12}C ratios of individual compounds in North Sea oils. Organic Geochemistry 21, 737–750.
Dahl, J.E.P., Moldowan, J.M., Peters, K.E., Claypool, G.E., Rooney, M.A., Michael, G.E., Mello, M.R., Kohnen, M.L., 1999. Diamondoid hydrocarbons as indicators of natural oil cracking. Nature 399, 54–61.
Dahl, J.E.P., Liu, S., Carlson, R.M.K., 2003. Isolation and structure of higher diamondoids, nanometer-sized diamond molecules. Science 299, 96–99.
Deng, S., Zhao, R., Kong, Q., Li, Y., Li, B., 2022. Two distinct strike-slip fault networks in the Shunbei area and its surroundings, Tarim Basin: hydrocarbon accumulation, distribution, and controlling factors. AAPG Bulletin 106, 77–102.
Fang, C., Xiong, Y., Li, Y., Chen, Y., Liu, J., Zhang, H., Adedosu, T.A., Peng, P., 2013. The origin and evolution of adamantanes and diamantanes in petroleum. Geochimica et Cosmochimica Acta 120, 109–120.
Graas, G.W., 1990. Biomarker maturity parameters for high maturities: calibration of the working range up to the oil/condensate threshold. Organic Geochemistry 16, 1025–1032.
Grice, K., Alexander, R., Kagi, R., 2000. Diamondoid hydrocarbon ratios as indicators of biodegradation in Australian crude oils. Organic Geochemistry 31, 67–73.

Guo, C., Chen, D., Qing, H., Dong, S., Li, G., Wang, D., Qian, Y., Liu, C., 2016. Multiple dolomitization and later hydrothermal alteration on the Upper Cambrian-lower Ordovician carbonates in the northern Tarim Basin, China. Marine and Petroleum Geology 72, 295–316.

He, T., Zeng, Q., Lu, S., Li, W., Li, M., Wen, Z., Yang, E., Jing, T., Ying, J., Zhu, P., Wang, X., Pan, W., Zhang, B., Chen, Z., 2023. Aryl isoprenoids from the Lower Paleozoic in the Tarim Basin, NW China: insight into deep ancient hydrocarbon exploration. Geoenergy Science and Engineering 225, 211666.

Li, S., Amrani, A., Pang, X., Yang, H., Said-Ahmad, W., Zhang, B., Pang, Q., 2015. Origin and quantitative source assessment of deep oils in the Tazhong Uplift, Tarim Basin. Organic Geochemistry 78, 531–553.

Li, K., Cai, C., Tan, X., Jiang, H., Fan, J., 2022. Multiple fluid flow events and diversity of hydrothermal minerals in Neoproterozoic to lower Paleozoic carbonate reservoirs, Tarim Basin, NW China. Journal of Asian Earth Sciences 233, 105260.

Li, H., Gao, J., Cao, Z., Zhu, X., Guo, X., Zeng, S., 2023. Spatial-temporal distribution of fluid activities and its significance for hydrocarbon accumulation in the strike-slip fault zones, Shuntuoguole low-uplift, Tarim Basin. Earth Science Frontier 30, 316–328 (in Chinese with English abstract).

Li, S., Pang, X., Jin, Z., Yang, H., Xiao, Z., Gu, Q., Zhang, B., 2010b. Petroleum source in the Tazhong Uplift, Tarim Basin: new insights from geochemical and fluid inclusion data. Organic Geochemistry 41, 531–553.

Li, M., Wang, T., Chen, J., He, F., Yun, L., Akbar, S., Zhang, W., 2010a. Paleo-heat flow evolution of the Tabei uplift in Tarim Basin, northwest China. Journal of Asian Earth Sciences 37, 52–66.

Li, M., Wang, T.-G., Lillis, P.G., Wang, C., Shi, S., 2012. The significance of 24-norcholestanes, triaromatic steroids and dinosteroids in oils and Cambrian-Ordovician source rocks from the cratonic region of the Tarim Basin, NW China. Applied Geochemistry 27, 1643–1654.

Li, Y., Xiong, Y., Chen, Y., Tang, Y., 2014. The effect of evaporation on the concentration and distribution of diamondoids in oils. Organic Geochemistry 69, 88–97.

Lin, R., Wilk, Z.A., 1995. Natural occurrence of tetramantane ($C_{22}H_{28}$), pentamantane ($C_{26}H_{32}$) and hexamantane ($C_{30}H_{36}$) in a deep petroleum reservoir. Fuel 74, 1512–1521.

Machel, H.G., Krouse, H.R., Sassen, R., 1995. Products and distinguishing criteria of bacterial and thermochemical sulfate reduction. Applied Geochemistry 10, 373–389.

Mango, F.D., 1997. The light hydrocarbons in petroleum: a critical review. Organic Geochemistry 26, 417–440.

Moldowan, J.M., Dahl, J., Zinniker, D., Barbanti, S.M., 2015. Underutilized advanced geochemical technologies for oil and gas exploration and production-1. The diamondoids. Journal of Petroleum Science and Engineering 126, 87–96.

Orr, W.L., 1974. Changes in sulfur content and isotopic ratios of sulfur during petroleum maturation—study of Big Horn Basin Paleozoic oils. AAPG Bulletin 58, 2295–2318.

Peng, Y., Cai, C., Fang, C., Wu, L., Liu, D., Sun, P., Liu, D., 2022. Diamondoids and thiadiamondoids generated from hydrothermal pyrolysis of crude oil and TSR experiments. Scientific Reports 12, 196.

Qiao, R., Chen, Z., 2022. Petroleum phase evolution at high temperature: a combined study of oil cracking experiment and deep oil in Dongying Depression, eastern China. Fuel 326, 124978.

Qiao, R., Chen, Z., Li, C., Wang, D., Gao, Y., Zhao, L., Li, Y., Liu, J., 2022. Geochemistry and accumulation of petroleum in deep lacustrine reservoirs: a case study of Dongying Depression, Bohai Bay Basin. Journal of Petroleum Science and Engineering 213, 110433.

Qiao, R., Li, M., Zhang, D., Xiao, H., 2024a. Geochemistry and accumulation of the ultra-deep Ordovician oils in the Shunbei oilfield, Tarim Basin: coupling of reservoir secondary processes and filling events. Marine and Petroleum Geology 167, 106959.

Qiao, R., Li, M., Zhang, D., Xiao, H., 2024b. Evaporative fractionation as the important formation mechanism of light oil reservoirs in the Dongying Depression, NE China. Energies 17, 3734.

Scarlett, A.G., Spaak, G., Mohamed, S., Plet, C., Grice, K., 2019. Comparison of tri-, tetra- and pentacyclic caged hydrocarbons in Australian crude oils and condensates. Organic Geochemistry 127, 115–123.

Schimmelmann, A., Lewan, M.D., Wintsch, R.P., 1999. D/H isotope ratios of kerogen, bitumen, oil, and water in hydrous pyrolysis of source rocks containing kerogen types I, II, IIS, and III. Geochimica et Cosmochimica Acta 63, 3751–3766.

Schulz, L.K., Wilhelms, A., Rein, E., Steen, A.S., 2001. Application of diamondoids to distinguish source rock facies. Organic Geochemistry 32, 365–375.

Song, H., Chen, M., Dou, L., Cheng, D., Wen, Z., 2024. Effects of biodegradation on diamondoid distribution in crude oils from the Bongor Basin. Chad. Energy Geoscience 5, 100260.

Song, D., Zhang, C., Li, S., Wang, T., Li, M., 2017. Elevated mango's K_1 values resulting from thermochemical sulfate reduction within the Tazhong oils, Tarim Basin. Energy & Fuels 31, 1250–1258.

Wang, D., Cai, C., Yun, L., Liu, J., Sun, P., Jiang, Z., Peng, Y., Zhang, H., Wei, T., Pei, B., 2023. Controls on petroleum stability in deep and hot reservoirs: a case study from the Tarim Basin. Marine and Petroleum Geology 147, 106014.

Wang, Q., Hao, F., Cao, Z., Tian, J., Cong, F., 2021. Geochemistry and origin of the ultra-deep Ordovician oils in the Shunbei field, Tarim Basin, China: implications on alteration and mixing. Marine and Petroleum Geology 123, 104725.

Wang, D., Kutuzov, I., Zhang, H., Cao, Z., Wang, Q., Amrani, A., Cai, C., 2024a. Application of sulfur isotopes of volatile organic sulfur compounds to determine the natural gas secondary alterations and possible sources in the Tarim Basin, NW China. Marine and Petroleum Geology 169, 107078.

Wang, R., Zhu, G., Wang, T., Wen, Z., Zhu, Y., Zhang, Z., 2024b. Identification of new higher diamondoids in condensate, their elution patterns, and mechanisms: a case study from Well ZS1C, Tarim Basin. Energy & Fuels 38, 14009–14024.

Wei, Z., Moldowan, J.M., Fago, F., Dahl, J.E., Cai, C., Peters, K.E., 2007. Origins of thiadiamondoids and diamondoidthiols in petroleum. Energy & Fuels 21, 3431–3436.

Wei, Z., Mankiewicz, P., Walters, C., Qian, K., Phan, N.T., Madincea, M.E., Nguyen, P.T. H., 2011. Natural occurrence of higher thiadiamondoids and diamondoidthiols in a deep petroleum reservoir in the Mobile Bay gas field. Organic Geochemistry 42, 121–133.

Wingert, W.S., 1992. GC–MS analysis of diamondoid hydrocarbons in Smackover petroleums. Fuel 71, 37–43.

Xu, H., Liu, Q., Zhu, D., Peng, W., Meng, Q., Wang, J., Shi, J., Jin, Z., 2022. Molecular evidence reveals the presence of hydrothermal effect on ultra-deep-preserved organic compounds. Chemical Geology 608, 121045.

Xu, H., Liu, Q., Jin, Z., Zhu, D., Meng, Q., Wu, X., Li, P., Zhu, B., 2024. Organic compounds in geological hydrothermal systems: a critical review of molecular transformation and distribution. Earth-Science Reviews 252, 104757.

Zhang, S., Su, J., Wang, X., Zhu, G., Yang, H., Liu, K., Li, Z., 2011. Geochemistry of Palaeozoic marine petroleum from the Tarim Basin, NW China: Part 3. Thermal cracking of liquid hydrocarbons and gas washing as the major mechanisms for deep gas condensate accumulations. Organic Geochemistry 42, 1394–1410.

Zhu, G., Wang, R., Wang, T., Wen, Z., Zhang, Z., 2023. Identification of thiadiamondoids in oil samples from Tazhong Uplift, Tarim Basin. Earth Science 48, 98–412 (in Chinese with English abstract).